J. Fluid Mech. (1970), *vol.* 40, *part* 4, *pp.* 783–806
Printed in Great Britain

The effects of gravity modulation on the stability of a heated fluid layer

By P. M. GRESHO AND R. L. SANI
Department of Chemistry and Chemical Engineering, University of Illinois

(Received 19 May 1969 and in revised form 18 September 1969)

The stability of a horizontal layer of fluid heated from above or below is examined for the case of a time-dependent buoyancy force which is generated by shaking the fluid layer, thus causing a sinusoidal modulation of the gravitational field. A linearized stability analysis is performed to show that gravity modulation can significantly affect the stability limits of the system. In this analysis, much emphasis is placed on qualitative results obtained by an approximate solution, which permits a rather complete stability analysis. A useful mechanical analogy is developed by considering the effects of gravity modulation on a simple pendulum. Finally, some effects of finite amplitude flows are considered and discussed.

1. Introduction

It is well known that if a quiescent fluid layer is heated uniformly from below, the adverse density gradient becomes unstable and fluid motion ensues when a critical heating rate, measured in terms of the Rayleigh number, is exceeded. A comprehensive review of this stability problem is given in Chandrasekhar (1961). If, however, the heating rate (or some other influencing parameter) is time-dependent, the classical stability analysis no longer applies. For example, if one or both of the bounding surface temperatures is sinusoidally varied about a steady heating rate, it has been shown (Venezian 1969) that the stability limit of the system is changed; temperature modulation may be a stabilizing or a destabilizing influence. A somewhat related system, the flow between concentric, rotating cylinders (Taylor instability), has been investigated experimentally by Donnelly (1964) and analytically by Meister & Münzner (1966) when the inner cylinder is sinusoidally modulated. The modulation was shown to be a stabilizing influence over the parameter range studied. Also, Rosenblat (1968) found that modulation could have a stabilizing or destabilizing effect on a class of time-periodic, inviscid flows.

In this paper we examine the stability of a heated fluid layer in which the gravitational field consists of a constant part plus a sinusoidally varying part; this modulation of gravity may be realized by vertically oscillating a fluid layer in a constant gravitational field. The effect of gravity modulation on the existence of standing waves on the free surface of a liquid in a vessel was analyzed by Benjamin & Ursell (1954); their analysis, like ours, was centred around the stability characteristics of Mathieu's equation. An approximate linear stability analysis

is performed in order to assess the qualitative effects of gravity modulation, considering both heating from below and the normally uninteresting case of heating from above. A simple pendulum analogy, the stability characteristics of which are known, is shown to apply to the fluid layer system. The effect of the modulation on the flow pattern and heat transfer rate is then considered by retaining the non-linear terms in the governing equations. These finite amplitude effects are analyzed only for two-dimensional roll cells of a single wave-number.

2. Development of equations

The system to be considered consists of a thin layer of Newtonian fluid heated uniformly and steadily from above, or below; the fluid is confined between two large, rigid horizontal plates which are sinusoidally oscillated in the vertical direction (parallel to the gravitational field). The usual Boussinesq approximations (Chandrasekhar) are invoked, and a linear dependence of density upon temperature is assumed. The initial quiescent state whose stability is questionable is characterized by a linear temperature and parabolic pressure distribution between the plates at any instant in time.

It is convenient to study the behaviour of the system from a Cartesian reference frame fixed on the top plate (the z-direction is vertically down), such that the plate oscillations are manifest by simply a sinusoidal modulation of the gravitational force. The dimensionless equations governing such a system are

$$\left(\frac{\partial}{\partial t}-\nabla^2\right)\theta = -\sqrt{|R|}\, w - \mathbf{u}.\nabla\theta, \tag{1}$$

$$\left(\frac{1}{Pr}\frac{\partial}{\partial t}-\nabla^2\right)\nabla^2 w = \mp\sqrt{|R|}\,(1+\epsilon\sin\omega t)\nabla_2^2\theta+\frac{1}{Pr}\bar{N}, \tag{2}$$

where

$$\nabla_2^2 = \frac{\partial^2}{\partial x^2}+\frac{\partial^2}{\partial y^2}.$$

The dimensional transformation is as follows: time is in units of h^2/κ; length is in units of the layer depth h; temperature is in units of the overall temperature difference ΔT, divided by the square root of the Rayleigh number

$$R = \gamma\Delta T g h^3/\kappa\nu;$$

velocity is in units of κ/h. Here γ is the volumetric coefficient of thermal expansion, g is the acceleration due to gravity, κ is the thermal diffusity, and ν is the kinematic viscosity. The Prandtl number is $Pr = \nu/\kappa$, $\mathbf{u}$ is the velocity, w is the vertical component of velocity, and θ is the temperature deviation from the linear profile; the actual temperature is given by $T = \Delta T(z+\theta/\sqrt{|R|})$. Finally, ω is the (dimensionless) frequency of the oscillation and ϵ is a measure of the amplitude of oscillation in 'units of g'; i.e. ϵ is the dimensionless acceleration and is given by $\epsilon = \delta Fr\omega^2$, where $Fr = \kappa^2/gh^3$ is a sort of Froude number based on the characteristic velocity κ/h. The non-linear terms are $\mathbf{u}.\nabla\theta$ (convective energy transport) and $\bar{N}$ (related to the convective acceleration $\mathbf{u}.\nabla\mathbf{u}$ in the Navier–Stokes equation); the explicit form of $\bar{N}$ need not be presented since it will vanish identically in the simplified treatment considered in this work.

Also, in (2) the minus sign applies to a layer heated from below (the normal scheme with $\Delta T > 0$), while the plus sign applies to a layer heated from above, a normally stable arrangement, with $\Delta T < 0$.

The boundary conditions in the vertical direction are those for rigid, conducting walls:

$$\theta = w = \partial w/\partial z = 0 \quad \text{at} \quad z = 0, 1. \tag{3}$$

No boundary conditions are imposed in the lateral directions, and initial conditions are unimportant, since we will be interested in the long time behaviour of systems with large lateral dimensions.

The solution to (1) and (2) will be assumed to consist of two-dimensional roll cells of a single wave-number α; the size of these periodic cells is $\lambda = 2\pi/\alpha$. The solution will be obtained approximately using Galerkin's method (Finlayson & Scriven 1966) with time-dependent amplitude coefficients. The Nth order approximate solutions are represented by

$$w = \cos\alpha x \sin\pi z \sum_{i=1}^{N} V_i(t) \sin(2i-1)\pi z, \tag{4}$$

$$\theta = \sum_{i=1}^{N} \overline{T}_i(t) \sin 2i\pi z + \cos\alpha x \sum_{i=1}^{N} T_i(t) \sin(2i-1)\pi z. \tag{5}$$

The roll cell is described by the $\cos\alpha x$ term. The first part of the temperature representation describes the distortion of the linear conduction profile caused by convection. The factor of 2 in the sine functions assures the same heat flow at both top and bottom surfaces. The second part of the temperature representation, sometimes called the perturbation temperature, is dependent on lateral position and has zero horizontal mean. The Nusselt number is the ratio of the heat transfer with convection present to that with no flow and is given by

$$Nu = 1 + \frac{1}{\sqrt{|R|}} \frac{\partial\bar{\theta}}{\partial z}\bigg|_{z=0}, \tag{6}$$

where the bar indicates a horizontal average. From (5)

$$Nu = 1 + \frac{2\pi}{\sqrt{|R|}} \sum_{i=1}^{N} i\overline{T}_i(t). \tag{7}$$

Finally, it is noteworthy that only the even-symmetry class (even about the midplane, $z = \frac{1}{2}$) of sine functions has been employed for the velocity and temperature perturbations. The even and odd symmetry classes are not coupled for this system and can thus be examined independently. The even mode is associated with the lowest Rayleigh number for which the system is unstable and the solutions describe a single cell between the two surfaces. Even at very large Rayleigh numbers, wherein a solution with two cells in the vertical direction is also possible (the odd solution), it is expected that the even solution will dominate and only one cell would be observed. In fact, all of the sine functions were included in certain representative cases and the above behaviour was substantiated. The equations

for the amplitude coefficients which are generated by Galerkin's method are (the dot represents a time derivative):

$$\dot{\bar{T}}_i = -i^2\pi^2\bar{T}_i + \sum_{m=1}^{N}\sum_{n=1}^{N} A_{nmi}V_m(t)\,T_n(t), \tag{8}$$

$$\dot{T}_i = -(i^2\pi^2+\alpha^2)\,T_i + 2\sqrt{|R|}\sum_{j=1}^{N} B_{ij}V_j(t) - 2\sum_{m=1}^{N}\sum_{n=1}^{N} A_{imn}V_m(t)\,\bar{T}_n(t), \tag{9}$$

and

$$\sum_{j=1}^{N}\{C_{ij}\dot{V}_j(t) + Pr\,[D_{ij}.V_j(t) \pm \alpha^2\sqrt{|R|}(1+\epsilon\sin\omega t).B_{ij}T_j(t)]\} = 0, \quad \text{for } i = 1, 2, \ldots, N \tag{10}$$

(the + sign in (10) is for $R > 0$). The coefficient matrices are defined in the appendix.

Note that the only non-linear terms present for the single wave-number analysis result from the term $\mathbf{u}.\nabla\theta$ in (1); there are no non-zero contributions from the term represented by $\bar{N}$ in (2). In effect, then, the only non-linear interactions allowed are those involving the horizontally averaged temperature field. If harmonics of $\cos\alpha x$ were employed, there would result additional non-linear interactions in the energy equation, and the term $\bar{N}$ in (2) would contribute non-zero terms. Since this work is in the nature of an exploratory effort, the more approximate description of the roll cells seems justified. Further, it is expected that the higher harmonics of $\cos\alpha x$ will generally be unimportant when the Rayleigh number is not far from its critical value; the validity of this assumption may be surmised from the results of Veronis (1966) for steady heating with no modulation. Future plans, however, do include examining the effects of higher harmonics of $\cos\alpha x$; these will be published separately (Gresho 1969).

Upon inverting the C_{ij} matrix, (10) is converted to the form (8) and (9); the entire set of $3N$ first-order equations can then be integrated simultaneously (e.g. via a fourth-order Runge–Kutta technique).

3. Linearized approximation using one trial function: comparison with a simple pendulum

Although the non-linear terms in (8) and (9) are required if finite amplitude effects are significant, they may be dropped if one is interested only in the limits of stability as described by the linearized equations; for such a stability analysis, (8) may be omitted completely and the last term in (9) may be neglected. Further, a reasonable first approximation may be realized by using only one trial function ($N = 1$). In this case (9) and (10) become

$$\dot{T}_1 = -(\pi^2+\alpha^2)\,T_1(t) + 2\sqrt{|R|}\,B_{11}V_1(t), \tag{11}$$

$$\dot{V}_1 = -\frac{Pr}{C_{11}}[D_{11}V_1(t) \pm \alpha^2\sqrt{|R|}(1+\epsilon\sin\omega t)\,B_{11}T_1(t)]. \tag{12}$$

Eliminating $V_1(t)$ between (11) and (12) gives (dropping subscripts)

$$\ddot{T} + 2p\dot{T} - f(\beta)\,Pr\,[(R-R_0) + \epsilon R\sin\omega t]\,T = 0, \tag{13}$$

where $$\beta = \alpha^2/\pi^2,$$

$$2p = (\pi^2+\alpha^2)+Pr.D/C = \pi^2\left[(1+\beta)+Pr.\frac{(16+8\beta+3\beta^2)}{4+3\beta}\right],$$

$$f(\beta) = 2\alpha^2B^2/C = \frac{256}{9\pi^2}\frac{\beta}{4+3\beta},$$

and $$R_0 = \frac{-D(\pi^2+\alpha^2)}{2\alpha^2B^2} = \frac{9\pi^6}{256}\frac{(1+\beta)(16+8\beta+3\beta^2)}{\beta}.$$

R_0 is the normal ('no shake') critical Rayleigh number; for these trial functions, $R_0 = 1824{\cdot}8$ at the critical wave-number ($\alpha = 3{\cdot}117$) whereas the exact result for this system is 1707·8 (Chandrasekhar), thus providing some measure of the error to be expected using only one trial function. Equation (13) is valid for both positive and negative Rayleigh numbers.

At this point we introduce a mechanical analogue to the fluid layer system; viz. a simple pendulum with viscous damping whose pivot point is sinusoidally oscillated in the vertical direction. The equation of motion for such a pendulum of length l is

$$\ddot{\theta}+2\xi\omega_0\dot{\theta} \pm \left(\omega_0^2+2\xi\omega_0\omega\frac{\delta}{l}\cos\omega t-\omega^2\frac{\delta}{l}\sin\omega t\right)\theta = 0. \tag{14}$$

This equation is valid for planar motion at small angles θ from the vertical. The vertical motion of the pivot is given by $\delta\sin\omega t$. Also, $\omega_0 = \sqrt{(g/l)}$ is the undamped natural frequency and ξ is the damping ratio. The plus sign applies to the normal, hanging pendulum and the negative sign to the statically unstable, inverted pendulum. The evident analogy is thus: the temperature of an oscillating fluid layer may be likened to the motion of a simple pendulum wherein exist two quite different modes for each system (a fluid heated from below ($R > 0$) is 'top heavy', as is an inverted pendulum); while a fluid heated from above ($R < 0$) is statically stable, as is a hanging pendulum. Since it is well known (Den Hartog 1940; Stoker 1950; Cunningham 1958) that vertical oscillations of the pivot point can (i) destabilize a statically stable, hanging pendulum and (ii) stabilize a statically unstable inverted pendulum†, it seems quite reasonable to expect gravity modulation to have a similar effect on a heated fluid layer. Although this analogy was drawn using a one-term approximation to w and θ, the results so obtained were always found to be qualitatively valid for larger values of N. Further support for the validity may be obtained by considering the (mathematically popular) so-called 'free-free' boundary conditions on w. Although such an experiment would be twice as difficult (for $\epsilon > 1$) as the 'no shake' system in the laboratory, it nevertheless relates to some of the principal features of the physically realizable system while being much simpler to analyze.

† The physical explanation of these phenomena is based on energy considerations. A hanging pendulum is destabilized by oscillation if the phase angle between the input and the response is such as to add a net amount of energy to the system. This energy addition is obtained, in part, by performing work against the centrifugal force (mv^2/r) during the part of the cycle when v^2 is large and by removing energy through the same force when v^2 is small. Similar reasoning applies to the inverted pendulum, which must have a net amount of energy removed if it is to be stabilized.

Specifically, with a linear conduction temperature profile, a free-free system has an exact solution of the form $w = V(t)\cos\alpha x \sin\pi z$ and $\theta = T(t)\cos\alpha x \sin\pi z$ (in the linearized approximation). This system leads directly to equations similar to (11), (12), and (13), all of which would be 'exact' up to this point.

Thus the stability predictions to be obtained using one trial function may be taken to be qualitatively correct but quantitatively approximate; e.g. with respect to (1) the location of a boundary between stable and an unstable solution and (2) the exact value of the critical Rayleigh number and wave-number at a point of marginal stability.

Both (13) and (14) can be cast into the canonical form of the Mathieu equation, which is (McLachlan 1964)

$$\ddot{X} + (a + 2q\cos 2\tau)X = 0. \tag{15}$$

The solution to this equation is of the form $X = F(\tau)e^{\mu\tau}$ where $F(\tau)$ is a periodic function with period π or 2π and μ is the characteristic, or Floquet, exponent, which is in general a complex function of a and q. The special case $\mu = 0$ results in a class of solutions called Mathieu functions; for each Mathieu function there is a unique relationship between a and q (one of which may be considered as an eigenvalue of (15) for a given value of the other). The regions in the a–q plane separated by the Mathieu functions are alternately stable and unstable

$$(Re(\mu) < 0 \quad \text{and} \quad > 0, \text{ respectively}),$$

with the boundaries being neutrally stable. There are solutions to (15) both for $a > 0$ and $a < 0$; also, q may be replaced by $-q$ with no effect on the solutions.

After changing variables, the Mathieu parameters a and q are related to those in (13) and (14) as follows: For the pendulum, $\frac{1}{2}q = \delta/l$ and (i) $2/\sqrt{a} = \omega/\omega_0(1-\xi^2)^{\frac{1}{2}}$ for the underdamped ($\xi < 1$) hanging pendulum, (ii) $2/\sqrt{-a} = \omega/\omega_0(\xi^2-1)^{\frac{1}{2}}$ for the overdamped ($\xi > 1$) hanging pendulum, and (iii) $2/\sqrt{-a} = \omega/\omega_0(1+\xi^2)^{\frac{1}{2}}$ for the inverted pendulum. For the fluid layer the corresponding relationships are $\frac{1}{2}q = f(\beta)\,Pr\,R\epsilon/\omega^2 = f(\beta)\,Pr\,R\delta\,Fr = f(\beta).\delta.(\gamma\Delta T)$; this implies that the roll cell behaves as a pendulum with an effective (dimensionless) length of $1/f(\beta)\,\gamma\Delta T$, a 'quite long' pendulum, since $\gamma\Delta T = \Delta\rho/\rho$ is usually much less than unity. Also, $2/\sqrt{a} = \omega/(f(\beta)\,Pr(R_N - R))^{\frac{1}{2}}$ for $R < R_N$ and $2/\sqrt{-a} = \omega/(f(\beta)\,Pr\,(R - R_N))^{\frac{1}{2}}$ for $R > R_N$, where R_N is termed the negative critical Rayleigh number ($R_N < 0$) and is a function of Pr and β; for the trial functions employed here R_N is given by

$$R_N = -R_0(\beta).\frac{(F(\beta).Pr - 1)^2}{4F(\beta)\,Pr}, \tag{16}$$

where

$$F(\beta) = \frac{16 + 8\beta + 3\beta^2}{(4+3\beta)(1+\beta)}$$

and R_0 is the previously defined critical Rayleigh number with no gravity oscillation. The negative critical Rayleigh number defines the dividing line between monotonic decay (real growth rate) and damped oscillatory decay (complex growth rate) for the 'no-shake' system; for $R_N < R < R_0$, the decay is monotonic while for $R < R_N$ the decay is damped oscillatory. This behaviour also has a direct analogue with the pendulum model: $R > 0$ corresponds to the inverted

pendulum, $R_N \leqslant R < 0$ corresponds to the overdamped, hanging pendulum, and $R < R_N$ corresponds to the underdamped, hanging pendulum.

The damping terms in (13) and (14) have a stabilizing influence on the solutions, i.e. the exponential behaviour is no longer given by $e^{\mu t}$. For the pendulum, the argument of the exponential factor is $(\frac{1}{2}\mu.\omega/\omega_0 - \xi)\omega_0 t$ and the stability

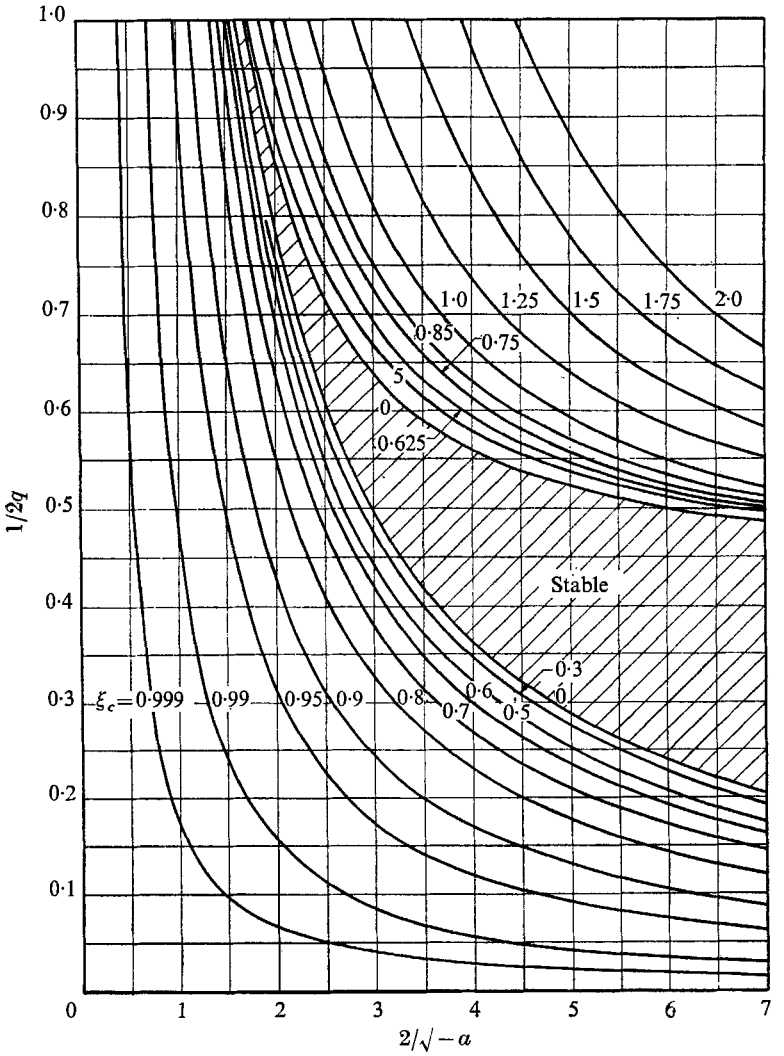

FIGURE 1. Stability chart for Mathieu equation: $-a$ plane.

criterion is seen to be $\xi \geqslant \frac{1}{2}\mu.\omega/\omega_0$. Hence the pendulum stability depends on the amount of damping present, the frequency ratio ω/ω_0, and the characteristic exponent of Mathieu's equation. In the stable regions of Mathieu's equation, μ is complex with a negative real part; hence in these regions even an undamped ($\xi = 0$) pendulum is stable. For the fluid layer, the exponential factor is $(\frac{1}{2}\mu\omega - p)t$ and the stability criterion is $p \geqslant \frac{1}{2}\mu\omega$. Here, since μ is a function of a and q and

these in turn depend on R, Pr, β, ϵ, and ω, the fluid layer stability is seen to depend, as expected, on these same parameters.

Although there are limited values of $\mu(a, q)$ available (Abramovitz & Stegun 1964; McLachlan 1964) no comprehensive data could be located. Hence, in order readily to assess the stability of this system (in terms of the parameters of interest,

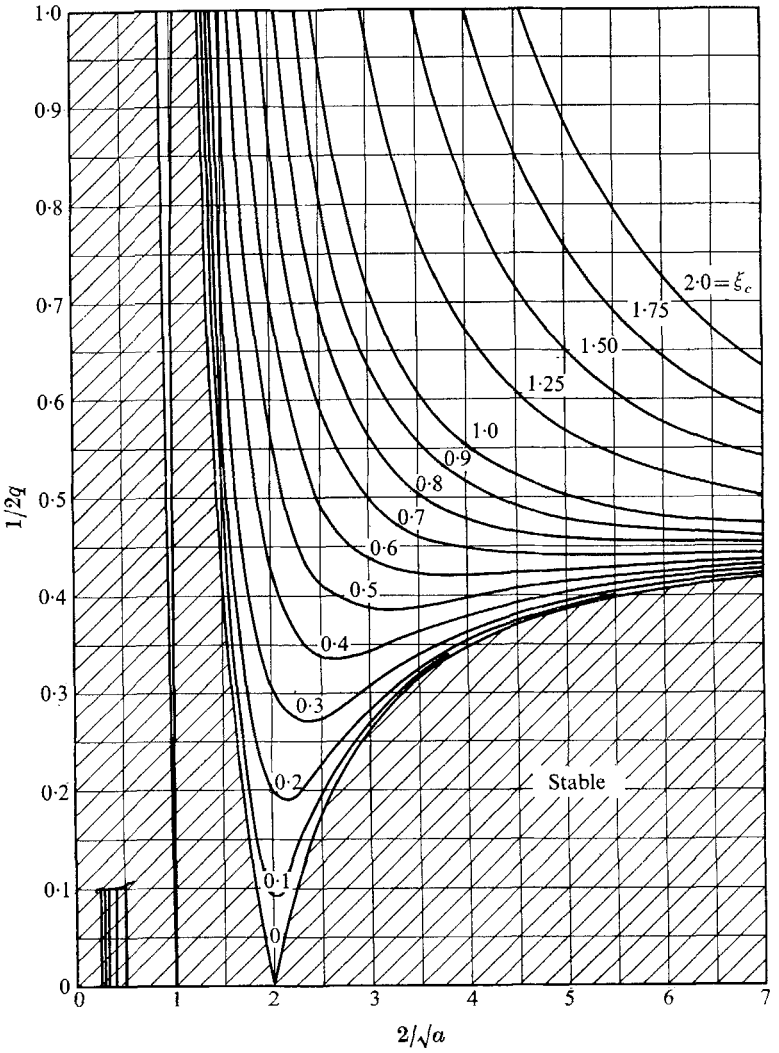

FIGURE 2. Stability chart for Mathieu equation: $+a$ plane.

viz. $\frac{1}{2}q$ and $2\sqrt{\pm a}$), the first task was to compute 'Mathieu stability charts' for both positive and negative values of a. This was done by numerically integrating Mathieu's equation from 0 to π for many values of a and q, following the method outlined in Abramovitz & Stegun. For this purpose, it was found more convenient to utilize a modified form of the characteristic exponent, viz. $\xi_c = \mu/\sqrt{\pm a}$. Values of ξ_c *vs.* $\frac{1}{2}q$ and $2\sqrt{\pm a}$ are shown in figure 1 for $a < 0$ ($R > R_N$) and in figure 2 for $a > 0$ ($R < R_N$). In each figure, the shaded regions correspond to

stable solutions of Mathieu's equation, while the other regions give unstable solutions. The lines of constant ξ_c are seen to appropriately enlarge the stable regions owing to damping effects. In terms of the new parameter ξ_c, the stability criteria for the fluid layer become:

(i) for $R > R_N$ (use figure 1): stable for $R \leqslant R_m$, where

$$R_m = R_N + (R_0 - R_N)/\xi_c^2; \tag{17}$$

(ii) for $R < R_N$ (use figure 2): stable for $R \geqslant R_m$, where

$$R_m = R_N - (R_0 - R_N)/\xi_c^2. \tag{18}$$

For $R = R_m$, the layer is marginally stable. It should also be noted that there are alternate regions of synchronous response (solution has frequency ω) and subharmonic response (solution has frequency $\frac{1}{2}\omega$) depending on the location of the 'operating point' on the stability charts. Specifically, the first unstable region in figure 1 will give rise to synchronous response, while the second unstable region (for large q) in figure 1 and the entire (large) unstable region in figure 2 will produce subharmonic response. Finally, it should be mentioned that figures 1 and 2 represent only limited, but most significant, portions of the overall stability plot (cf. McLachlan, for example).

4. Results and discussion

The analysis was performed in the following manner: (i) The stability charts were used to obtain an 'overall stability map' of the system corresponding to the crude, one-trial function approximation. (ii) A number of 'spot checks' were made by comparing specific results from (i) with those employing up to five trial functions. (iii) Finite amplitude (i.e. non-linear) effects were studied, again first with only one trial function, and finally (iv) certain of these non-linear results were 'confirmed' by showing at least qualitative agreement when compared to those obtained using five trial functions.

4·1. *Linear stability analysis*

(i) *Qualitative results using one trial function.* Figures 1 and 2 may be utilized to determine the critical Rayleigh number as a function of the shaking parameters, ω and δFr (note that Fr depends on the fluid property κ). The critical Rayleigh number is defined, at fixed ω, δFr, Pr, (*a*) for $R > R_N$, as that Rayleigh number above which the system is unstable, and (*b*) for $R < R_N$, as that Rayleigh number below which the system is unstable. Note that this definition, as usual, implies the existence of a critical, or 'most dangerous', wave-number. In order to obtain R_c and α_c, many curves such as figure 3 were constructed, each at a different wave-number, the lowest such curve at a given ω defining R_c and α_c. Each point on figure 3 was obtained from figure 1 (for fixed Pr and δFr) as follows: (*a*) select a value of ξ_c, (*b*) compute R_m from (17), (*c*) compute $\frac{1}{2}q = f(\beta)\, Pr\, R_m \delta Fr$, (*d*) read $2/\sqrt{-a}$ from figure 1, and finally (*e*) compute the frequency from

$$2/\sqrt{-a} = \omega/(f(\beta)\, Pr(R_m - R_N))^{\frac{1}{2}}.$$

The resulting curve shows the region of stability for the given wave-number. The interesting 'neck' in the stable region of figure 3, while indeed stable for the wave-number in question, 'disappears' when the stability to all wave-numbers is examined. A similar procedure, employing figure 2, is used to determine R_c and α_c for the case of heating from above, where $R < R_N$. Figures 4 and 5 show the resulting critical Rayleigh number R_c and the associated critical wave-number α_c as a function of ω for $Pr = 7$ and $\delta Fr = 10^{-5}$.

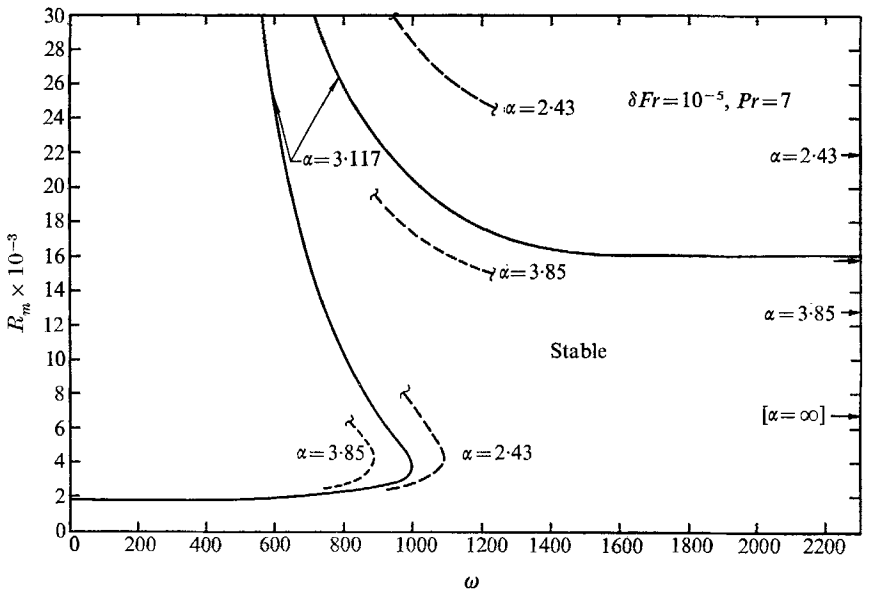

FIGURE 3. The marginally stable Rayleigh number at fixed α, Pr, and δFr.

Figure 4, for a fluid layer heated from below, shows that gravity modulation significantly increases the stability limit of this system. The effect is small at low frequencies, but becomes quite significant at higher frequency. The discontinuity at $\omega \cong 1250$ is caused by passing from the first unstable region to the second one in figure 1. As ω is increased through this point, the following abrupt changes are predicted: (*a*) R_c changes from a rapidly increasing function of ω to a slowly decreasing one, (*b*) the critical wave-number jumps from a small value (large roll cells) to a large one (its derivative with respect to ω also changes sign), and (*c*) the system response (i.e. w and θ) changes from synchronous to subharmonic. As ω is further increased, R_c approaches a limit which is a function of Pr and δFr $[R_c(\omega \to \infty) \cong 6770\,(7/Pr)\,(10^{-5}/\delta Fr)]$ but α_c continues to increase. If δFr is decreased, the R_c *vs.* ω curve would shift to the right and the peak value of R_c (as well as the asymptotic value) would increase. This also indicates that R_c may become less than R_0 at large δFr and high frequency. Thus the stability limit of the fluid layer is most strongly increased at small shaking amplitude and large shaking frequency; there is ostensibly no upper limit on the Rayleigh number which can be stabilized in this manner.

In figure 5 is shown a similar plot for a fluid layer heated from above. These

results, derived from the stability plot of figure 2, show that gravity modulation can destabilize a statically stable system if the heating rate is sufficiently high. In this figure, there are no quantitative results for $\omega < \sim 400$ since the unstable regions from a plot such as figure 2 become very small and $|R_c|$ becomes very large. A reasonable conjecture would be that for low frequencies, it would be almost impossible to destabilize a fluid which is heated from above. The interesting behaviour again occurs at high frequency. For $\omega > \sim 422$, the layer exhibits

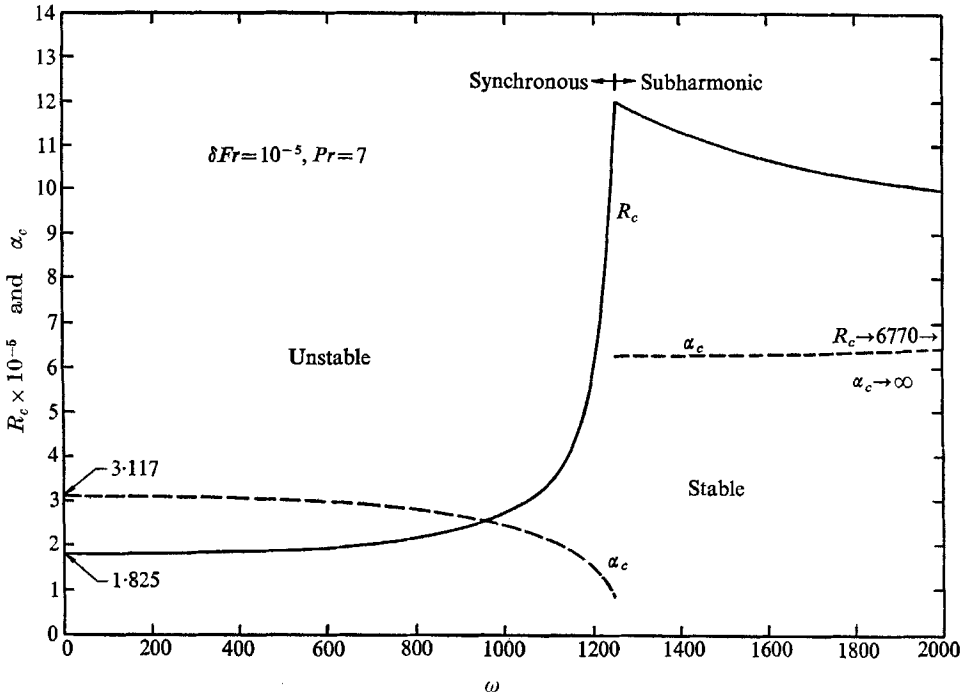

FIGURE 4. Critical Rayleigh number and wave-number for $R > R_N$, $Pr = 7$, $\delta Fr = 10^{-5}$ $(N = 1)$.

subharmonic response; as $\omega \to \infty$, $R_c \to -8508$ and $\alpha_c \to 7{\cdot}15$ for this Pr, δFr combination. If δFr is increased, the R_c *vs.* ω curves in figure 5 would shift downward and to the left, thus indicating that it is easier to destabilize the system if the shaking amplitude is large. Again, this analysis predicts that any negative Rayleigh number (such that $R < R_N$) can be destabilized by gravity modulation.

Finally, it is also predicted from figure 1, for $R_N < R < R_0$, that the fluid layer may be stable or unstable, depending on the frequency and amplitude of modulation. To summarize, any Rayleigh number other than zero can exhibit stability or instability for the proper combinations of δ and ω.

It may be instructive at this point to relate the dimensionless parameters to those for some 'real' experiment. The following frequencies (in cycles/sec) correspond to $\omega = 1000$: (*A*) for $h = 1$ cm; 250 for hydrogen gas, 35 for air, 7·4 for liquid mercury, 0·227 for water, and 0·16 for a typical silicone oil. (*B*) For $h = 0{\cdot}1$ cm, increase the above values by a factor of 100. The 'Froude number',

$Fr = \kappa^2/gh^3$ for the above liquids is: (A) For $h = 1$ cm; 250×10^{-5} for hydrogen, 5×10^{-5} for air, $0{\cdot}22 \times 10^{-5}$ for mercury, $0{\cdot}00021 \times 10^{-5}$ for water, and $0{\cdot}0001 \times 10^{-5}$ for silicone oil. (B) for $h = 0{\cdot}1$ cm, increase the above values by a factor of 1000. Thus, for example, a 1 mm layer of water ($Pr = 7$) will have $\delta Fr = 10^{-5}$ if $\delta = 4{\cdot}8$; also, at $\omega = 1000$, the frequency is 22·7 cycles per second and the peak acceleration is $\epsilon = \delta Fr\omega^2 = 10$ g's.

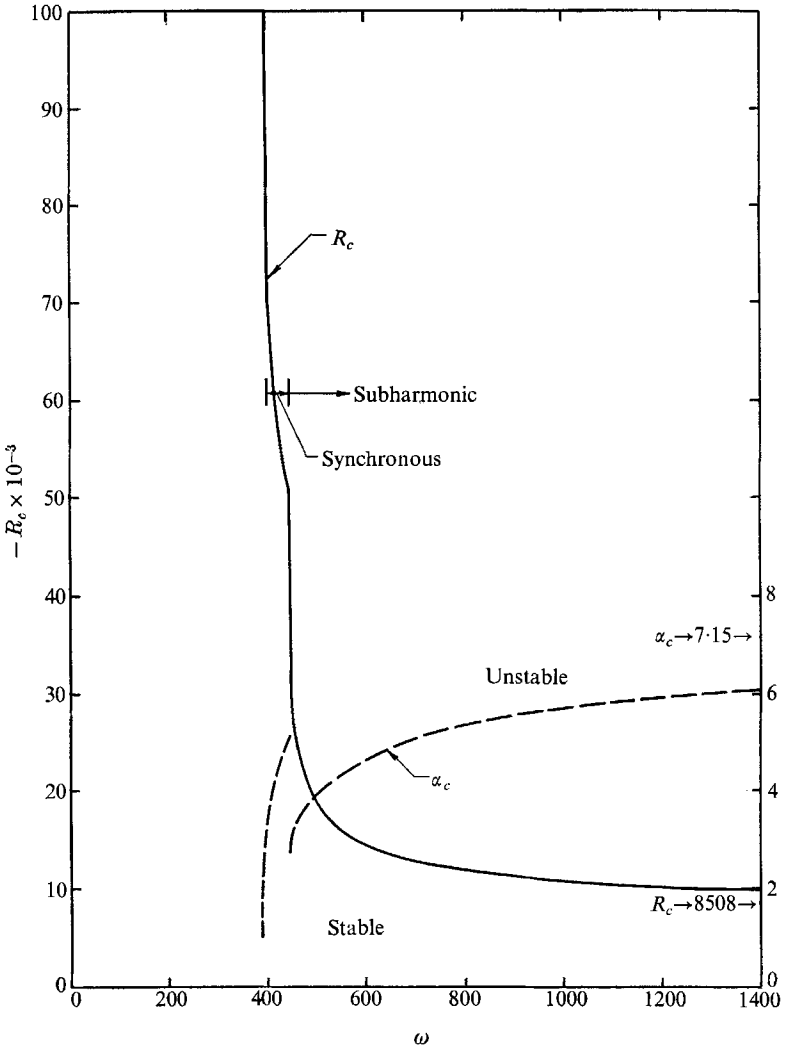

FIGURE 5. Critical Rayleigh number and wave-number for $R < R_N$, $Pr = 7$, $\delta Fr = 10^{-5}$ ($N = 1$).

(ii) *The effect of additional trial functions.* Many runs were made using the computer program in order to check (a) the accuracy of the graphical analysis via the stability charts (i.e. $N = 1$) and (b) the adequacy of the approximation based on trial function ($N = 3$, 4, or 5). In general it was found that the error introduced by the graphical analysis was of the same order of magnitude (2–10 % or so) as

that when comparing $N = 5$ to $N = 1$. Also, in all cases examined, the difference between $N = 4$ and $N = 5$ was quite small; thus $N = 5$ was taken as an 'upper limit'. (For $N = 5$, $R_0 = 1710{\cdot}1$ for $\alpha = 3{\cdot}117$ compared to the exact value of $R_0 = 1707{\cdot}8$). As an example let us consider two points on figure 4; $R_c \cong 3400$ at $\omega = 1100$ and $R_c \cong 10{,}300$ at $\omega = 1800$ were obtained graphically. These two points were checked with the computer program using $N = 1$ and $N = 5$; all parameters from figure 4 were fixed except the Rayleigh number. The results are as follows: at $\omega = 1100$, the critical Rayleigh number is ~ 3090 with $N = 1$, and ~ 3120 with $N = 5$; at $\omega = 1800$, R_c is $\sim 10{,}500$ with $N = 1$, and $\sim 10{,}000$ with $N = 5$. Here the marginal state is obtained by plotting $V_1(t)$ or $C_1(t)$ *vs.* time on semi-logarithmic paper to obtain the growth rate for a given R; a second plot of growth rate *vs.* R yields the marginal state at zero growth rate. The very close agreement in the first case between $N = 1$ and $N = 5$ is probably somewhat fortuitous; these checks do instill a reasonable degree of confidence in the approximate, graphical analysis, however,

4·2. *Finite amplitude results*

Most non-linear results were also obtained using one trial function, with frequent 'spot checks' using five trial functions; again, the simplest description of the system proved to be qualitatively quite reliable. For this approximation, the momentum equation is one given by (12), the corresponding temperature perturbation is given by (11) with $\frac{16}{5}\, V.\overline{T}$ added to the right side; finally, the amplitude coefficient of the correction to the horizontal mean temperature is given by

$$\dot{\overline{T}} = -4\pi^2 \overline{T}(t) - \tfrac{8}{5} V(t).T(t). \tag{19}$$

Figure 6 shows some typical, long time, synchronous results with heating from below. Both sets of curves are for $Pr = 7$ and $\omega = 800$; the solid curves are for $R = 10^4$, $\alpha = 3{\cdot}44$ and $\epsilon = 5{\cdot}7$ ($\delta Fr = 8{\cdot}9 \times 10^{-6}$) and the dashed curves correspond to $R = 3000$, $\alpha = 2{\cdot}82$ and $\epsilon = 6{\cdot}4$ ($\delta Fr = 10^{-5}$). For the first case, the marginally stable Rayleigh numbers are ~ 2240 and $\sim 12{,}300$, the higher value of R_m corresponding to the 'neck' region of figure 3. The corresponding steady solution for $\omega = 0$ ('no shake' solution) is $V = 27{\cdot}1$, $T = -19{\cdot}7$, and $\overline{T} = 21{\cdot}6$ ($Nu = 2{\cdot}36$). For the second case, the marginally stable Rayleigh numbers are ~ 2260 and 10,300, and the 'no shake' solution is $V = 9{\cdot}26$, $T = -14{\cdot}9$, and $\overline{T} = 5{\cdot}58$ ($Nu = 1{\cdot}64$). The results displayed in figure 6 indicate that, to this order of approximation, the velocity is more strongly affected by the modulation than is the temperature. It is also seen that the velocity is of opposite sign for a small part of the cycle, indicating that the roll cells (i.e. the particle paths along the streamlines) actually reverse direction, but still display a net rotation in one direction. Even under conditions of marginal stability (e.g. by increasing δ for the first case, and decreasing δ for the second case, to reach the nearest stable region) the roll cells would rotate farther in one direction than the other; mathematically this is explained by the occurrence of 'constant terms' in some of the Mathieu functions. The physical explanation is less straightforward: the only way that oscillations can remove energy from this (synchronous) system (i.e. inverted pendulum) is if there exists a permanent 'offset'.

For example, in the pendulum system, if θ_0 is the constant pendulum offset angle, the net energy transferred to support is approximately proportional to $\sin\theta_0$.

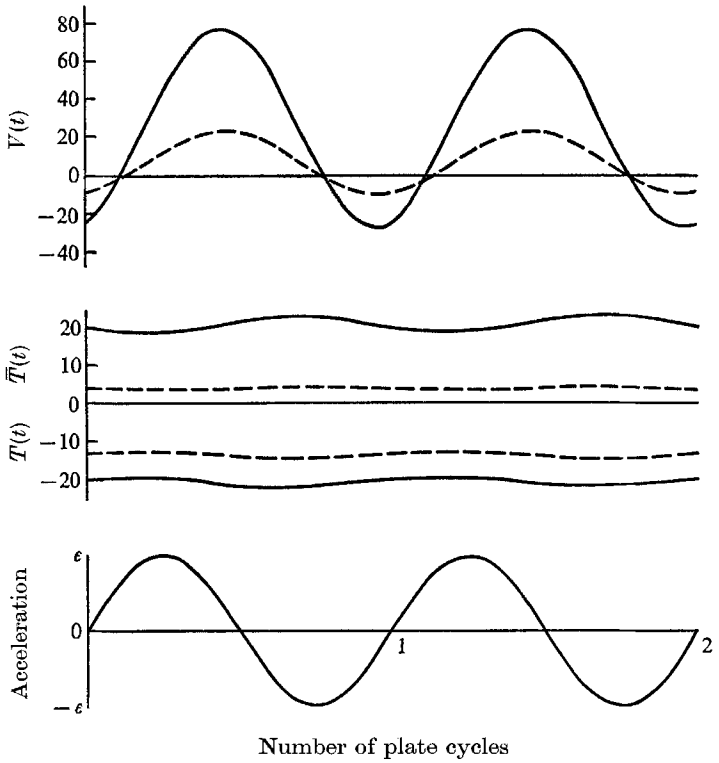

FIGURE 6. Amplitude coefficients ($N = 1$) showing synchronous response with heating from below: $Pr = 7$, $\omega = 800$. ——, $R = 10^4$, $\alpha = 3{\cdot}44$, $\epsilon = 5{\cdot}7$; – – –, $R = 3000$, $\alpha = 2{\cdot}82$, $\epsilon = 6{\cdot}4$.

In figure 7 is shown a similar result except that ϵ, ω are adjusted to give subharmonic response. For this case, $R = 10^4$, $Pr = 7$, $\alpha = 6{\cdot}66$, $\omega = 1332$ (the fluid responds at a frequency of 666) and $\epsilon = 21{\cdot}2$ ($\delta Fr \cong 1{\cdot}2 \times 10^{-5}$). The steady solution for no modulation is $V = 21{\cdot}9$, $T = -16{\cdot}0$, $\overline{T} = 14{\cdot}2$ ($Nu = 1{\cdot}89$) and the marginally stable Rayleigh number with modulation is ~ 9500. In this case, the oscillation is seen to have even more dramatic effects, the most significant of which is that there is no net flow: the fluid particles move the same distance in each direction, completing one cycle each time the plates complete two cycles. Again, the shapes of the curves are not unlike Mathieu functions; here the solution would be comprised of Mathieu-type functions, which have no 'constant term', at least for $V(t)$ and $T(t)$. Note, however, that the heat flux temperature coefficient $\overline{T}(t)$ still contains a constant part, and that it responds at the higher, forcing frequency. It is also noteworthy that the heat flux is generally much less than the 'no-shake' value and 'peaks' as w goes through zero for all cases exhibiting subharmonic response. Finally, let us briefly compare these results to those obtained using more trial functions. First, the qualitative features of the

solution are identical, with the higher-order terms tending (in all cases studied) to increase the fluid velocity. With one trial function, the following maximum values were obtained: $V_1 \cong 64{\cdot}5$, $T_1 \cong 8{\cdot}7$, $\bar{T}_1 \cong 1{\cdot}24$ (Nu varies from 1·03 to 1·08). With two trial functions for V_i and T_i, but one for $\bar{T}_i$, we obtain: $V_1 \cong 112$, $T_1 \cong 14$, and $\bar{T}_1 \cong 3{\cdot}6$ (Nu varies from 1·10 to 1·23). Finally with five trial functions for V_i, T_i and four for $\bar{T}_i$ we obtain: $V_1 \cong 132$, $T_1 \cong 16$, $\bar{T}_1 \cong 4{\cdot}4$ (Nu varies from 1·15 to 1·21). Also, for this last case, V_2 has a maximum value of ~ 26, $V_3 \cong 8$, $V_4 \cong 2$, and $V_5 \cong 0{\cdot}8$; all of these higher-order velocity coefficients are approximately in phase with the principal coefficient V_1.

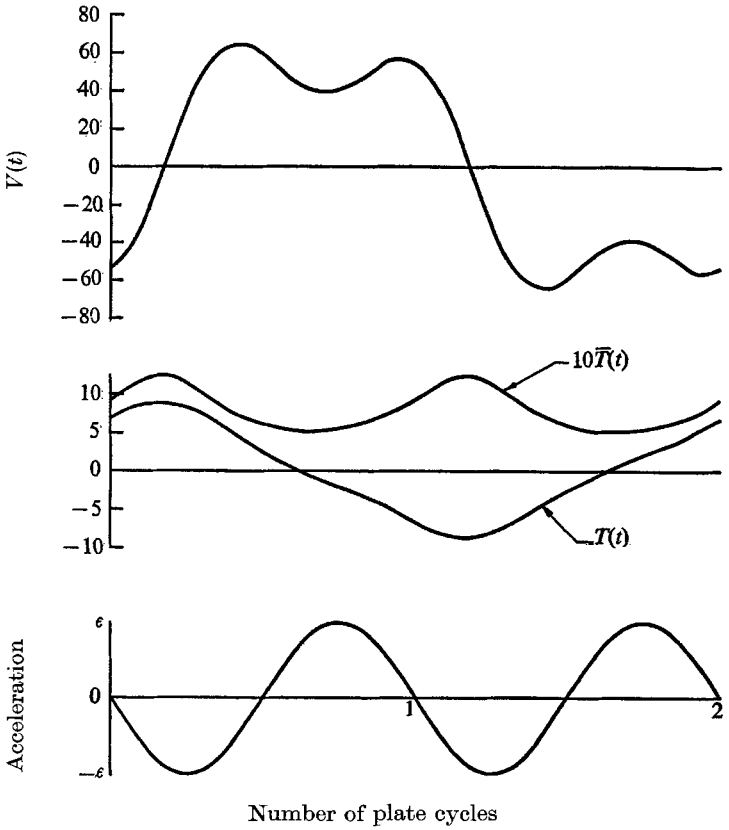

FIGURE 7. Amplitude coefficients ($N = 1$) showing subharmonic response with heating from below: $R = 10^4$, $Pr = 7$, $\alpha = 6{\cdot}66$, $\omega = 1332$, $\epsilon = 21{\cdot}2$.

A fluid layer heated from above will generally exhibit subharmonic response if it is destabilized by shaking and, in fact, the response will be qualitatively similar to that just discussed. Figure 8 shows the long-time response for $R = -14{,}985$, $Pr = 7, \alpha = 4{\cdot}97, \omega = 750$ and $\epsilon = 4{\cdot}82$ ($\delta Fr \cong 8{\cdot}6 \times 10^{-6}$). Under these conditions the marginally stable Rayleigh number is ~ -14230 and the solution with no modulation is, of course, zero.

Most of the non-linear 'exploratory' calculations were performed with an analogue computer using the one-term approximation. This allowed a rapid search for 'interesting' behaviour, which could later be checked by the digital

computer program using more trial functions. Another, very practical reason for relying on the analogue computer is that the non-linear interactions frequently cause the system to display very long term transient effects due to the initial conditions (and especially to the initial lack of proper phasing, in time, of the amplitude coefficients); typically 50–200 'plate cycles' are required to achieve a relatively steady, oscillatory solution (if one exists). These transient effects

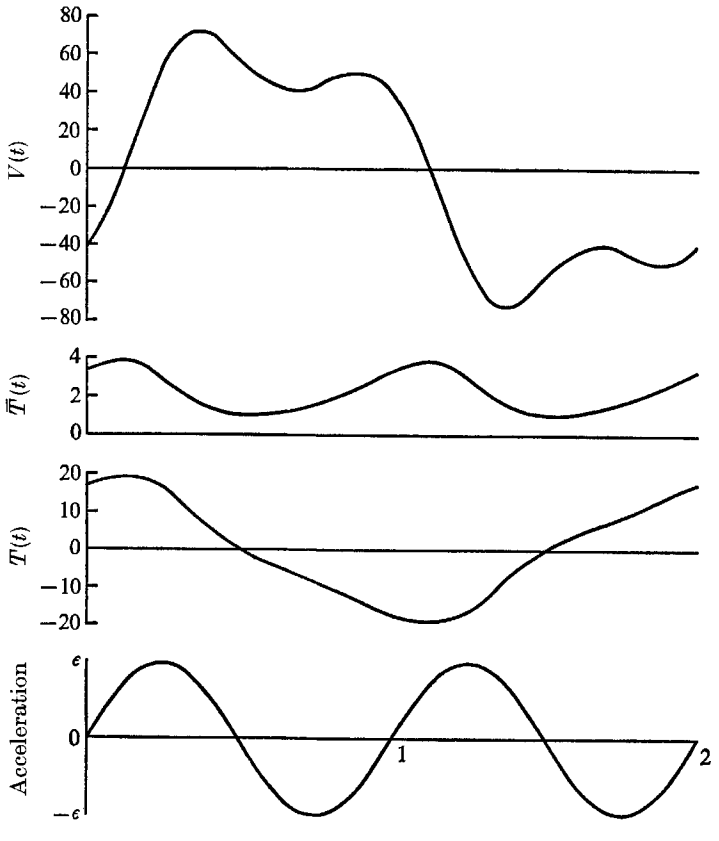

FIGURE 8. Amplitude coefficients ($N = 1$) showing subharmonic response with heating from above: $R = -14{,}985$, $Pr = 7$, $\alpha = 4{\cdot}97$, $\omega = 750$, $\epsilon = 4{\cdot}82$.

can be quite expensive when using the digital computer with several trial functions. Although the results presented here are among the most common 'solution types', there were many other interesting responses; e.g. at $R = 20{,}000$, $Pr = 7$, $\alpha = 3{\cdot}44$, $\omega = 800$ and $\epsilon = 4{\cdot}04$, the response was similar to that in figure 6 except that $V(t)$, and to a lesser extent $T(t)$ and $\bar{T}(t)$, were apparently modulated by a very low frequency wave ($\sim \frac{1}{8}$ of the forcing frequency). Some of these unusual wave forms will be published separately (Gresho).

We will, however, present one example of the most unusual type of response encountered; the so-called 'relaxation oscillation'. The data for figure 9 are identical to those for the first case of figure 6 except that the amplitude δ is a

factor of four larger ($\delta Fr = 3{\cdot}56 \times 10^{-5}$), thus raising the ordinate ($\frac{1}{2}q$) in figure 1 well into the second unstable region ($R_m \cong 5300$). This relaxation-type of oscillation was observed many times, for both $R > 0$ and $R < 0$ (always in the subharmonic region at large acceleration ϵ) and was never found to be exactly periodic

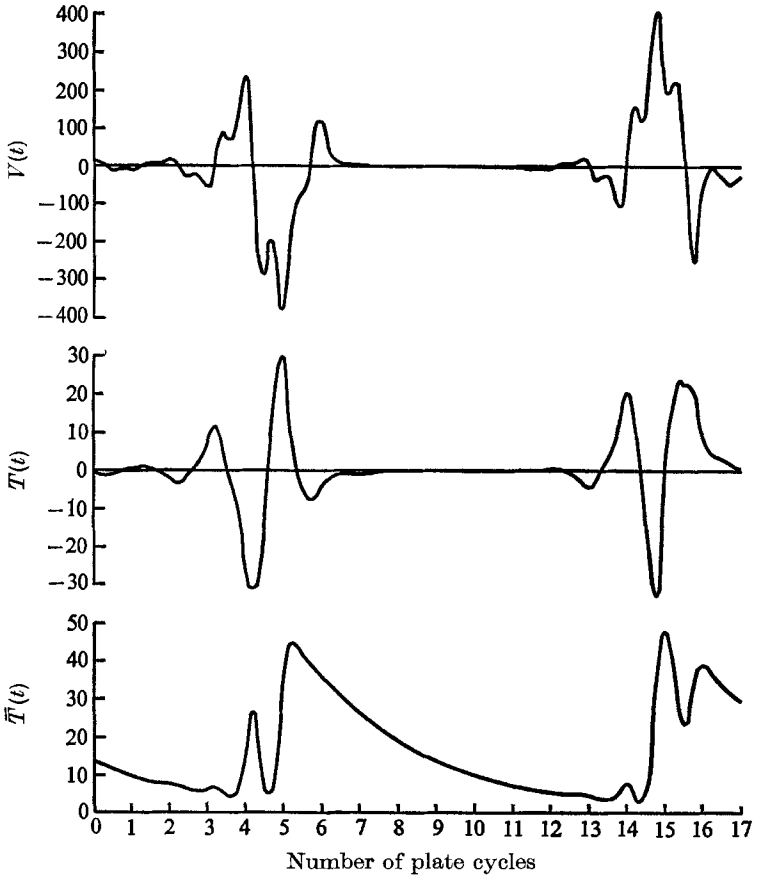

FIGURE 9. Amplitude coefficients ($N = 1$) showing relaxation oscillations; $R = 10^4$, $Pr = 7$, $\alpha = 3{\cdot}44$, $\omega = 800$, $\epsilon = 22{\cdot}8$.

although the number of 'plate cycles' between the explosive bursts (~ 10 in figure 9) was relatively consistent for a given run. (It is also noteworthy that the occurrence of (periodic) relaxation oscillations in a heated fluid layer with no shaking has been predicted by Busse 1967 in the case of a fluid layer supported by a conduction layer in which is maintained a given rate of heat production.)

A crude explanation of this phenomenon is offered here: When finite amplitude effects are small, the system is predicted to be highly unstable according to linear theory; hence the growth rate of the perturbations is very large and $V(t)$ and $T(t)$ grow rapidly as predicted by linear theory. Since $\bar{T}(t)$, the distortion of the horizontal temperature from a linear profile, grows according to the product of $V(t)$ and $T(t)$, the mean temperature profile will be little affected until $V(t)$ and $T(t)$ become fairly large; but, since they do so in a relatively short time span,

the effect on $\bar{T}(t)$ is almost one of a sudden 'impulse,' thus quickly causing $\dot{\bar{T}}(t)$ to become large and positive (since $V(t)$ and $T(t)$ are normally of opposite sign). Hence $\bar{T}(t)$ grows rapidly until thermal diffusion (the term $-4\pi^2\bar{T}(t)$ in (19)) again becomes significant and a balance is more or less restored: $\dot{\bar{T}}(t)$ goes to zero and finally changes sign. At this point we digress to reconsider the Mathieu parameters a and q, with non-linear interactions included. The result is (a) the ordinate, $\frac{1}{2}q$, must be multiplied by the factor $(1-\frac{6}{5}\pi\bar{T}/\sqrt{R})$ and (b) the abscissa, $2/\sqrt{-a}$, must be multiplied by the factor $[(R-R_N)/(R-R_N-\frac{6}{5}\pi\sqrt{R\bar{T}})]^{\frac{1}{2}}$. Since $\bar{T} > 0$, the non-linear interactions act to reduce the effective Rayleigh number; this causes the original point on figure 1 to move downward and to the right and possibly well into the shaded stable region. Although this reasoning is rigorous only if $\bar{T}(t)$ is constant, it nevertheless seems to apply to these relaxation oscillations where $\bar{T}(t)$ decays slowly. Thus it is postulated that when $\bar{T}(t)$ obtains some critical magnitude, the point on the stability chart (figure 1) moves into the stable region, causing $V(t)$ and $T(t)$ to decay rather quickly toward zero. Soon $V(t).T(t)$ becomes small compared to $4\pi^2\bar{T}$ and $\bar{T}$ is then acting as a disturbed, conduction temperature profile which slowly decays, or relaxes, as $e^{-4\pi^2 t}$, convection effects being negligible. As $\bar{T}(t)$ decays, however, the 'point of reckoning' on the stability chart gradually moves back upward and to the left. Eventually $\bar{T}(t)$ will be small enough so that the system again moves into the unstable region and the cycle begins anew.

This relaxation instability appears to be the most significant test of the 'credibility' of the simple model and was accordingly tested with five trial functions (four in $\bar{T}_i$) using the digital computer; the results, shown in figure 10 for some of the amplitude coefficients, again confirm the predictions of the simple model. The main differences between one and five trial functions for this case are as follows: (a) The peak velocity is larger than predicted with one trial function. (b) The heat transfer rate is also larger when more trial functions are employed: the maximum Nusselt number is $\sim 3{\cdot}7$ with $N = 1$ and $\sim 9{\cdot}7$ with $N = 5$. (c) The higher-order temperature coefficients are more significant than those for velocity. Finally, (d) there are only about seven plate cycles between 'bursts' with five trial functions, compared to about ten cycles with one trial function.

4·3. *Frozen-time approximation for low frequency*

For very low frequency ($\omega < \sim 1$), a 'frozen-time' model may be invoked on the basis that the growth rate of the perturbations is large compared to the rate of change of 'gravity' due to the modulation. The exponential growth rate factor with no modulation is then assumed to apply 'instantaneously' as follows (for heating from below),

$$\sigma = \omega_n \left[\left(\frac{R-R_N}{R_0-R_N} \right)^{\frac{1}{2}} - 1 \right], \tag{20}$$

where $R = R_m(1+\epsilon \sin \omega t)$ is considered here to be a slowly varying, time-dependent Rayleigh number: also $\omega_n^2 \equiv f(\beta)\, Pr(R_0-R_N)$. On this basis, the criterion for marginal stability must specify that there be no net growth or decay over one cycle; i.e.

$$\int_0^{2\pi/\omega} \sigma \, dt = 0. \tag{21}$$

Letting $\tau = \omega t$, the criterion for marginal stability becomes

$$2\pi \left(\frac{R_0 - R_N}{R_m - R_N}\right)^{\frac{1}{2}} = \int_0^{2\pi} (1 + k \sin \tau)^{\frac{1}{2}} \, d\tau, \tag{22}$$

where $k \equiv (\epsilon R_m / R_m - R_N) < 1$. Using the first three terms of the binomial expansion yields

$$|\epsilon| \cong 4 \frac{R_m - R_N}{R_m} \left(1 - \left(\frac{R_0 - R_N}{R_m - R_N}\right)^{\frac{1}{2}}\right)^{\frac{1}{2}}, \quad \text{for} \quad k \ll 1. \tag{23}$$

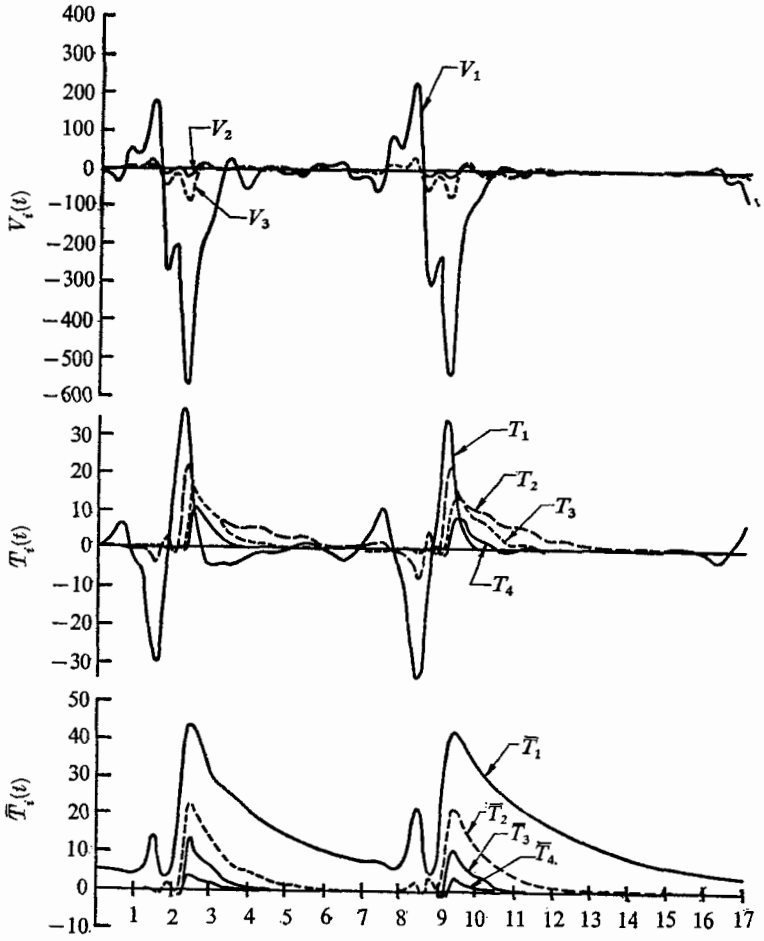

FIGURE 10. Amplitude coefficients ($N = 5$ for V_i, T_i; $N = 4$ for $\bar{T}_i$) showing relaxation oscillation with more trial functions; the parameter values are identical to those in figure 9.

Thus, for low frequency, the stability is defined not independently by δ and ω, but by the acceleration, $\epsilon = \delta Fr \omega^2$. The above relation was also obtained using asymptotic values ($\omega \to 0$) from the Mathieu stability chart.

Also, for $\omega < 1$, the above model applies quite well to the heated fluid layer in which one surface temperature is modulated sinusoidally about a mean value (cf. Venezian). The argument here is that, for very low frequency, the conduction

temperature profile can respond quickly enough so that there always exists a slowly varying, essentially linear temperature profile. In this case, ϵ is identified with the amplitude of the modulation, measured in terms of the nominal ΔT, and R_m is thus independent of ω. The frozen-time model may also be used to determine the effect of simultaneous oscillations in gravity and surface temperature. The results are: (*a*) for identical frequencies,

$$|\epsilon_T + \epsilon_g| = 4\frac{R_m - R_N}{R_m}\left(1 - \left(\frac{R_0 - R_N}{R_m - R_N}\right)^{\frac{1}{2}}\right)^{\frac{1}{2}}, \tag{24}$$

and (*b*) for different frequencies,

$$(\epsilon_T^2 + \epsilon_g^2)^{\frac{1}{2}} = 4\frac{R_m - R_N}{R_m}\left(1 - \left(\frac{R_0 - R_N}{R_m - R_N}\right)^{\frac{1}{2}}\right)^{\frac{1}{2}}. \tag{25}$$

From this it is seen that the effects ϵ_T and ϵ_g are simply additive when the frequencies are identical (e.g. if $\epsilon_g + \epsilon_T = 0$, the effects cancel and (24) gives $R_m = R_0$). For different frequencies however, the squares are additive and thus there is always enhancement of stability. Finally, it should be noted that one also obtains (23) for the case of free-free boundaries (with the corresponding definitions of R_0 and R_N, viz.

$$R_0 = \frac{(1+\beta)^3}{\beta}\pi^4, \quad R_N = -R_0\frac{(Pr-1)^2}{4Pr}.$$

For $\epsilon^2 \ll 8$, (23) can be inverted to give

$$R_m - R_0 \cong R_0 . \epsilon^2 \frac{Pr}{2(Pr+1)^2}. \tag{26}$$

This result is identical to the $\omega \to 0$ result obtained by Venezian using a perturbation analysis in ϵ. It is now seen to apply to temperature or gravity modulation (or both).

From the viewpoint of non-linear theory (or from an observational point of view in a laboratory), these low frequency results must be re-interpreted; for example, if $R_m = 5000$ and $\epsilon = 1$, it is clear (for $\omega \to 0$) that the system may be regarded as unstable during $\sim 71\,\%$ of the cycle (when $R > 1825$) and stable during the remaining 29 %, thus indicating that $\sigma < 0$ has a 'stronger influence' than the $\sigma > 0$ part of the cycle in (21). Now, in a non-linear experiment, given an arbitrary set of initial conditions at R_m, ϵ, one would find that the perturbations decay very slowly and would approach zero as $t \to \infty$ (the usual result from non-linear theory). This effect would probably not be observed in a laboratory experiment, however, owing to these 'ever-present, small perturbations', i.e.this system cannot be adequately described for all time by a unique set of initial conditions. Hence, in a laboratory, one would most likely observe flow during part of the cycle and no flow during the remainder of the cycle.Thus, for very low frequency oscillations, the usual mathematical description of the system (either linear or non-linear) may well generate spurious results in the sense of describing physical observations in the laboratory.

4·4. *Streamlines and particle paths*

It is of some interest to examine the details of the flow within the roll cells in order to compare the fluid motion to the motion of the plates. This will again be done approximately, using one trial function; this approximation should be reasonably good since $V_1(t)$ is quite dominant. Accordingly, the stream function for a roll cell is given by

$$\psi(x, z, t) = (1/\alpha)\, V(t) \sin \alpha x \sin^2 \pi z; \tag{27}$$

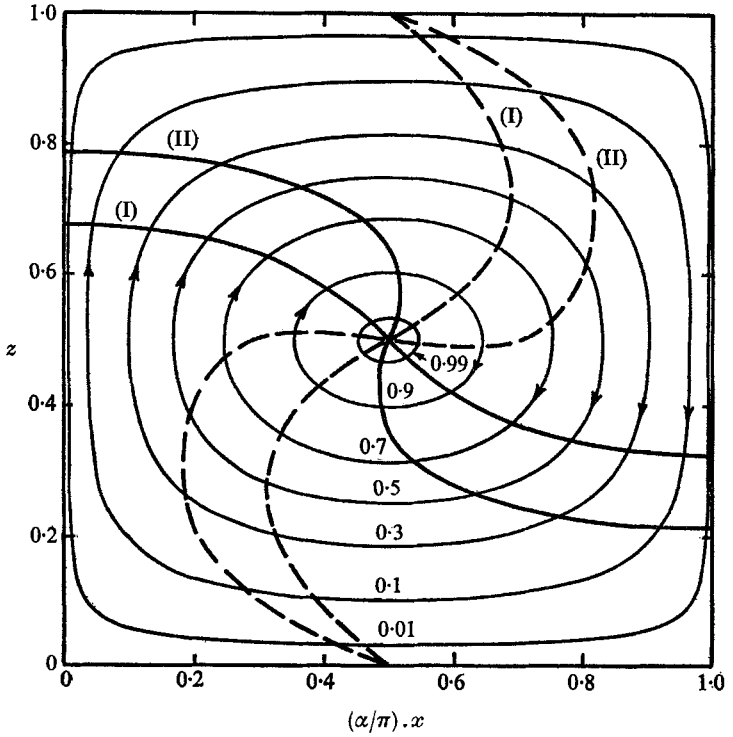

FIGURE 11. Streamlines and particle paths in a roll cell; —— curve is for the data of figure 6 (first case) and – – – curve for the data of figure 8.

the velocity components are $u = -\partial\psi/\partial z$, $w = \partial\psi/\partial x$. Since u and w contain the same time-dependent factor $V(t)$, the particle paths coincide with the streamlines (Aris 1962). The streamlines are obtained from $\sin \alpha x \sin^2 \pi z = c$ ($c < 1$) and are shown in figure 11 for several values of c. The motion of a fluid particle is obtained from $dx/u = dz/w = dt$ and the streamline equation, yielding, for our trial functions,

$$\int_0^t V(t)\, dt = \int_{z_0}^{z} \frac{dz}{(\sin^4 \pi z - c^2)^{\frac{1}{2}}} = \frac{\alpha}{2\pi\sqrt{c}} \int_{x_0}^{x} \frac{dx}{(\sin \alpha x - c)^{\frac{1}{2}}}. \tag{28}$$

The integral over t is performed numerically as $V(t)$ is computed, and the integral over x can be obtained in terms of incomplete elliptic integrals of the first kind.

Two cases will be presented here; the first is for the data of figure 6 (first case) and the second for the data of figure 8. For the former, the time integral of $V(t)\, dt$ over one plate cycle $2\pi/\omega$ is 0·20. In figure 11, the curves labelled (I) correspond to one plate cycle and those labelled (II) are for two plate cycles. The solid curves

were located along the line $z = 0{\cdot}5$ at $t = 0$, and the dashed curves were located at $\alpha x/\pi = 0{\cdot}5$ at $t = 0$; these curves represent the motion of the fluid particles, and may be visualized as if a dye streak were placed along $z = 0{\cdot}5$ and $x = 0{\cdot}5\pi/\alpha$ at $t = 0$. For this case of synchronous response, it is seen that the fluid particles traverse a fairly small portion of the total closed trajectory during one plate cycle, but that there is a net flow in one direction along the streamlines. The second example is one of subharmonic response at $R = -14{,}985$; for this case, the integral of $V(t)\,dt$ over one plate cycle is $\sim 0{\cdot}39$, and thus corresponds quite closely to the curves labelled (II) in figure 11. The key difference here is that there is no net flow (i.e. the integral of $V(t)\,dt$ over the next plate cycle is $\sim 0{\cdot}39$), and the dye streaks would return to their original locations at the end of two plate cycles. This oscillatory behaviour would also apply to a fluid heated from below, which is responding at half the forcing frequency, such as the case discussed in figure 7. While these oscillations seem fairly reasonable for a fluid layer heated from above (denser fluid below), they are much less obvious for the fluid heated from below, but then it is also far from obvious that an inverted pendulum can be stabilized by shaking.

5. Conclusions

(i) Gravity modulation can significantly affect the stability limits of a heated fluid layer. Specifically, (*a*) any positive Rayleigh number (heating from below) can be stabilized in some region of the δ–ω plane, with larger Rayleigh numbers being stabilized at high frequency and small amplitude. (*b*) Any negative Rayleigh number (heating from above) can be destabilized for some range of δ and ω, with high frequency and large amplitude being the most destabilizing.

(ii) With heating from below, there may occur two distinct types of flow patterns: (*a*) At low to moderate frequency, the response will be synchronous with the forcing frequency, and there will be net fluid motion along the streamlines, although there will be flow reversal during part of the cycle. The Nusselt number will usually be less than that with no modulation, since the modulation is a stabilizing influence. (*b*) At high frequency the response will be subharmonic, there will be no net flow along the streamlines, and the Nusselt number will be significantly lower than that with no modulation.

(iii) With heating from above, the flow pattern will be predominantly subharmonic with no net flow and rather low Nusselt number. There may exist a small range of intermediate frequency for which the flow response will be synchronous.

(iv) The Mathieu stability charts, which correspond to a one trial-function approximation, are quite useful in ascertaining the approximate stability limits with gravity modulation. One trial function also gives a reasonably good representation of finite-amplitude effects.

This research was supported in part by the National Science Foundation under Grant GP–287, which provided funds for the numerical computation, and in part by a fellowship received by P. M. G. from North American Rockwell Corporation.

Appendix

The coefficients in the Galerkin equations (8)–(10) are defined as follows, letting $f_i(z)$, $g_i(z)$, and $h_i(z)$ represent the ith trial functions for the vertical velocity, the temperature perturbation, and the mean horizontal temperature correction, respectively:

$$A_{ijk} = \int_0^1 g_i f_j \frac{dh_k}{dz} . dz,$$

$$B_{ij} = -\int_0^1 f_i g_i dz,$$

$$C_{ij} = -\int_0^1 \left(\frac{df_i}{dz}\frac{df_j}{dz} + \alpha^2 f_i f_j\right) dz,$$

$$D_{ij} = -\int_0^1 \left(\frac{d^2f_i}{dz^2}\frac{d^2f_j}{dz^2} + 2\alpha^2 \frac{df_i}{dz}\frac{df_j}{dz} + \alpha^4 f_i f_j\right) dz.$$

For the trial functions used here we have $f_i = \sin \pi z \sin (2i-1)\pi z$,

$$g_i = \sin (2i-1)\pi z, \quad \text{and} \quad h_i = \sin 2i\pi z;$$

letting $F_i = 2i-1$ yields

$$A_{ijk} = 4kF_iF_j\left\{\frac{2k-1}{[(2k-1)^2-(F_i^2+F_j^2)]^2-4F_i^2F_j^2} - \frac{2k+1}{[(2k+1)^2-(F_i^2+F_j^2)]^2-4F_i^2F_j^2}\right\},$$

$$B_{ij} = \frac{4}{\pi}\frac{F_iF_j}{1+F_i^4+F_j^4-2(F_i^2+F_j^2+F_i^2F_j^2)},$$

$$C_{ij} = \frac{\pi^2}{8}\{(1+\beta+F_iF_j)(\delta_{1|i-j|}-2\delta_{ij})-\beta\delta_{1i}\delta_{1j}\},$$

$$D_{ij} = \frac{\pi^4}{8}\{[(1+F_i^2)(1+F_j^2)+2\beta(1+F_iF_j)+\beta^2](\delta_{2|i-j|}-2\delta_{ij}) - 4(2F_iF_j\delta_{ij}+\delta_{1|i-j|})-\beta^2\delta_{1i}-\delta_{1j}\},$$

where $\delta_{1|i-j|} = 1$ for $|i-j| = 1$ and zero otherwise.

REFERENCES

Abramowitz, M. & Stegun, I. (eds.) 1964 *Handbook of Mathematical Functions with Formulas, Graphs, and Mathematical Tables*. U.S. Government Printing Office.

Aris, R. 1962 *Vectors, Tensors, and the Basic Equations of Fluid Mechanics*. Englewood Cliffs, N.J.: Prentice-Hall.

Benjamin, T. B. & Ursell, F. 1954 *Proc. Roy. Soc. Lond.* A **225**, 505.

Busse, F. H. 1967 *J. Fluid Mech.* **28**, 223.

Chandrasekhar, S. 1961 *Hydrodynamic and Hydromagnetic Stability*. Oxford University Press.

Cunningham, W. J. 1958 *Introduction to Nonlinear Analysis*. New York: McGraw-Hill.

Den Hartog, J. P. 1940 *Mechanical Vibrations* (2nd ed.). New York: McGraw-Hill.

Donnelly, R. J. 1964 *Proc. Roy. Soc. Lond.* A **281**, 130.

FINLAYSON, B. A. & SCRIVEN, L. E. 1966 *Applied Mech. Rev.* **19**, 735.

GRESHO, P. M. 1969 Ph.D. Thesis, University of Illinois.

MCLACHLAN, N. W. 1964 *Theory and Application of Mathieu Functions.* New York: Dover.

MEISTER, B. & MÜNZNER, W. W. 1966 *Z.A.M.P.* **17**, 537.

ROSENBLAT, S. 1968 *J. Fluid Mech.* **33**, 321.

STOKER, J. J. 1950 *Nonlinear Vibrations.* New York: Interscience.

VENEZIAN, G. 1969 *J. Fluid Mech.* **35**, 243.

VERONIS, G. 1966 *J. Fluid Mech.* **26**, 49.